Forest Change Mapping using Multi-Source Satellite SAR, Optical, and LiDAR Remote Sensing Data

Benyamin Hosseiny[1], Mahdieh Zaboli[1], Saeid Homayouni[2]

[1] School of Surveying and Geospatial Engineering, Faculty of Engineering, University of Tehran, Tehran, Iran - (ben.hosseiny, m_zaboli)@ut.ac.ir
[2] Centre Eau Terre Environnement, Institut National de la Recherche Scientifique, 490 Rue de la Couronne, Quebec City, QC G1K 9A9, Canada - saeid.homayouni@inrs.ca

Keywords: Deforestation, Canopy Height, GEDI, ICESat-2, Sentinel-1, Sentinel-2.

Abstract

This study highlights the efficacy of leveraging multi-source satellite remote sensing for precise and dependable forest change mapping. Forests play a crucial role as carbon reservoirs and are indispensable components of the global carbon and water cycle, providing essential ecosystem services. Despite their significance, forests face deforestation, diseases, and climate change threats. Recent satellite remote sensing technology advancements have facilitated accurate, persistent, and large-scale forest dynamics monitoring. New generation satellite LiDAR systems, such as GEDI and ICESat-2, offer frequent and global height information at high spatial resolutions. This research presents a processing framework for mapping forest changes by integrating SAR and optical features from Sentinel-1 and Sentinel-2 imagery with canopy heights derived from GEDI and ICESat-2 datasets. Multiple experiments and analyses were conducted in two study areas. The findings underscore the significant impact of incorporating canopy height information in enhancing the accuracy of forest change mapping, resulting in a 15% improvement in precision and a 13% enhancement in F1-score in the experimental setups. Furthermore, the developed model exhibits increased reliability and confidence in identifying correctly changed and unchanged areas while being less confident in incorrect predictions.

1. Introduction

Forests serve as vital carbon reservoirs integral to the global carbon and water cycle, offering essential ecosystem services. Despite their critical importance, forests are threatened by various factors such as deforestation, diseases, and climate change. Deforestation driven by agricultural expansion is the primary cause of forest loss and degradation, while mining, selective logging, fire, and road expansion are other drivers, all leading to a decline in forest biodiversity (Slagter et al., 2023; Vogt et al., 2019). Given the significant role of forests in global terrestrial carbon sink dynamics, accurate assessment of their changes is crucial for reducing uncertainties in carbon balance calculations. However, continuous monitoring of large forest areas is problematic due to the high costs. Remote sensing technology presents a solution by enabling timely and cost-effective forest dynamics monitoring.

Recent advances in remote sensing technology have enabled the accurate, persistent, and large-scale monitoring of forest changes. Notably, the free and open access data policy from satellite missions like the European Space Agency’s (ESA) Sentinel programme has fuelled significant research in Earth observation. The Sentinel-2 satellites, launched in 2015, carry multispectral optical sensors that provide high-resolution imagery (10-60 metres) across the visible, Near-Infrared (NIR), and Shortwave Infrared (SWIR) spectrum. These observations offer valuable insights into forest ecosystems, biology, and species. However, cloud cover, particularly during rainy seasons, can hinder the effectiveness of optical data. Synthetic aperture radar (SAR) data can overcome this limitation by penetrating clouds. The Sentinel-1 C-Band SAR sensor provides dual polarised VV-VH intensity images in Ground Range Detected (GRD) mode. This data ensures a consistent stream of dense time series data in high spatial detail, regardless of daylight or cloud cover conditions. One example of the effectiveness of Sentinel-1 data for forest monitoring is the near real-time Radar for Detecting Deforestation (RADD) alert system for detecting tropical forest disturbances (Reiche et al., 2021).

In addition to optical and radar satellites, a new generation of satellite LiDAR instruments, like the GEDI (Global Ecosystem Dynamics Investigation) onboard the International Space Station (ISS) and ATLAS (Advanced Topographic Laser Altimeter System) onboard ICESat-2, have emerged since around 2019, enabling high-resolution, global-scale height measurements. The GEDI mission utilises a waveform LiDAR instrument to sample forest heights with 25-metre diameter footprints every 60 metres along its orbital paths. It transmits 14 nanoseconds (4.2 metres) pulses of 1064 nanometre laser energy and records the returning waveform at a one nanosecond rate (approximately 0.15 meters) (Dubayah et al., 2020). GEDI’s canopy height products have proven effective in various Earth observation applications such as aboveground biomass estimation (Tamiminia et al., 2024), crop classification (Di Tommaso et al., 2021), and wetland mapping (Adeli et al., 2023). However, it is important to note that GEDI has been temporarily deactivated since March 2023, with a planned reactivation by the end of 2024.

ICESat-2, on the other hand, carries the Advanced Topographic Laser Altimeter System (ATLAS), which uses a green laser (532-nanometre wavelength) that transmits short 1.5 nanoseconds (approximately 0.4 metre) pulses at a 10 kHz frequency, resulting in along-track sampling of 0.7 metres (Neumann et al., 2019). The footprint diameter for each ATLAS laser pulse is estimated to be around 11 metres on the ground (Neumann et al., 2019). While ICESat-2’s primary mission focuses on ice sheet monitoring, its potential for forest height estimation has been demonstrated in several studies (Feng et al., 2023; Liu et al., 2021; Milenković et al., 2022).

Unlike SAR intensity product (GRD) and optical imagery, which provide radiometric and physical features that may not directly translate to forest height changes, LiDAR satellite missions offer

This contribution has been peer-reviewed. The double-blind peer-review was conducted on the basis of the full paper.
https://doi.org/10.5194/isprs-annals-X-4-2024-163-2024

a crucial geometrical feature: surface height measurement. This direct measurement allows for a more accurate assessment of changes in forest volume, making it a valuable tool for forest change monitoring.

This study has two primary objectives. First, we aim to demonstrate the effectiveness of multi-source satellite data for forest change monitoring. We achieve this by developing a framework that fuses three types of remotely sensed data, each offering unique characteristics and features. These data sources include spectral features from Sentinel-2 imagery (optical wavelength domain), backscattering features derived from Sentinel-1’s dual-polarised VV-VH C-band observations (SAR), and canopy height measurements acquired by GEDI and ATLAS laser scanners. Second, we investigated the impact of incorporating canopy height information into the feature set derived from optical and SAR data. Specifically, we analysed the effect of including height features on the model’s accuracy and assessed its influence on uncertainty.

2. Method

2.1 Data Processing

We extracted features from three domains: SAR, optical, and height, using data from four satellite sources: Sentinel-1, Sentinel-2, GEDI, and ATLAS.

2.1.1 Features from Sentinel-1 SAR data: We used Sentinel-1 dual-polarisation C-band data to extract SAR-related features. The Google Earth Engine (GEE) platform provides 10×10m resampled GRD data, and the terrain correction thermal noise removal has already been performed in GEE.

We extracted three prevalent features: Span, Ratio, and Radar Vegetation Index (RVI). Span (*VV+VH*), denoting the total backscatter coefficient, indicates the aggregate energy returned to the radar across VH and VV polarisation channels. Ratio highlights the backscattering power changes between two polarisations and is shown to be sensitive to vegetation dynamics and useful for biomass estimation. The dual-polarised RVI ($RVI = \frac{VH + VV}{4 \times VH}$), as an alternate representation of the full-polarised version (Kim and Zyl, 2009), aims to highlight vegetation density and is shown to be highly correlated with the Normalised Difference Vegetation Index (NDVI), while benefiting from not being affected by cloud cover (Mandal et al., 2020).

2.1.2 Features from Sentinel-2 Multispectral data: We derived three features highly sensitive to vegetation density and changes using Sentinel-2’s Red (R), NIR, and SWIR bands: Normalised Difference Vegetation Index (NDVI), Soil-Adjusted Vegetation Index (SAVI), and Normalized Burn Ratio (NBR). NDVI is highly sensitive to chlorophyll content, greenness, and health conditions in vegetation. SAVI, a modified version of NDVI, presents improved separability between vegetation and bare soil by adding soil adjustment factor (*L*) to the main equation. NBR ($NBR = \frac{NIR - SWIR}{NIR + SWIR}$), using the difference between the SWIR and NIR reflectance, is sensitive to vegetation loss and is, specifically, indicative of burned or severely disrupted zones.

2.1.3 Canopy Height: We leveraged canopy height products from two datasets: GEDI’s Level 2A (L2A) and ICESat-2 ATLAS ATL08. The GEDI L2A product provides detailed elevation and height metrics at the footprint level. These metrics are extracted from the received waveform, including terrain height, canopy height, and various relative height (RH) values (Dubayah et al., 2020). The RH values are provided at 1% intervals, from 0% to 100% per footprint, each representing the percentile of energy return height relative to the ground. To ensure data quality, we employed L2A’s “quality_flag” report to filter out unreliable or degraded GEDI data points.

The ATLAS ATL08 dataset contains terrain height estimates, canopy height estimates, and RH metrics describing the canopy’s vertical structure. Specifically, it provides three key canopy height metrics: “h_max_canopy” (maximum RH to the ground), “h_canopy” (98th percentile height), and “canopy_h_metrics” (percentiles from 10% to 95% relative to the interpolated ground surface with 5% intervals) (Neuenschwander et al., 2022).

We chose the RH98 metric (98th percentile) to represent canopy height in the GEDI data. Similarly, for ICESat-2 data, we utilised the “h_canopy” product, which is equivalent to the 98th percentile height (RH98). Several studies recommend the 98th percentile canopy height due to its reliability and less noisy canopy height estimation compared to the very top of the canopy (RH100) (Liu et al., 2021; Qi et al., 2023).

2.2 Modelling

We utilised a supervised machine learning approach to map forest changes using two series of data collected before and after the changes occurred. Random Forest (RF), known for its robustness, simplicity, and low sensitivity to hyperparameter tuning, is widely employed for modelling remote sensing data in various regression and classification applications. In addition to these attributes, RF can provide decision-making probabilities,

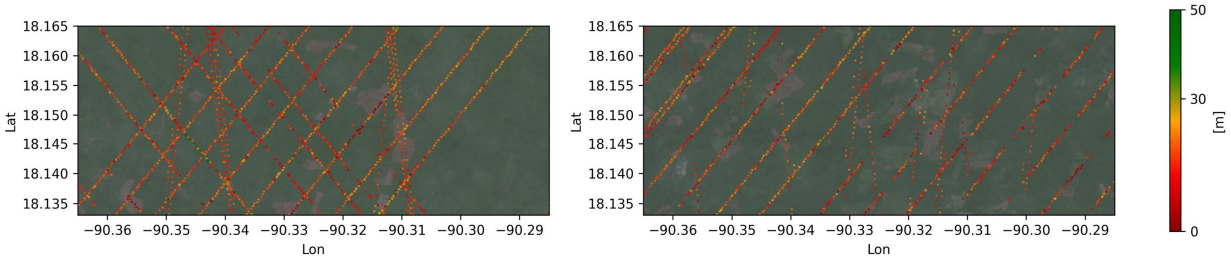

Figure 1: First study area located in Mexico: a) Before the changes, and b) After the changes. Slanted and near vertical patterns demonstrate height measurements by GEDI and ATLAS LiDARs, respectively.

estimated based on the votes from the multiple decision trees embedded and trained within the model.

We employed an RF Regression model to address the sparsity of GEDI and ATLAS canopy height data. This model created wall-to-wall canopy height layers with a 10m resolution. The model is trained using the canopy height data and corresponding pixel values in Sentinel-1 VV, VH intensity, and Sentinel-2 spectral bands. It then estimates the canopy height for other pixels in each scene. Subsequently, other feature layers described in the previous section were derived from the acquired Sentinel-1 and Sentinel-2 layers. The generated features from two data series were subtracted, and finally, the differentiated feature layers were used as input variables for the RF Classifier to classify pixels into changed and unchanged categories.

3. Data

We investigated deforestation in Mexico and Brazil, which have experienced significant disturbances recently. Specifically, we focused on the changes that occurred between 2020 and 2021. Satellite data collected in 2019 (pre-disturbance) and 2022 (post-disturbance) were used to identify deforested areas.

The ESA Worldcover Map 2020 (Zanaga et al., 2022) was used to mask non-forest areas. We refined an initial reference map from the RADD forest disturbance alert system (Reiche et al., 2021) by visually inspecting monthly high-resolution image mosaics (4.8 m spatial resolution) from Planet Imagery. Furthermore, disturbances occurring outside the 2020-2021 period were excluded.

The Sentinel-1, Sentinel-2, and GEDI L2A data were acquired and processed through Google Earth Engine (GEE) Python API, while the ATLAS ATL08 data were acquired from the NASA EarthData platform.

Figures 1 and 2 present Sentinel-2 RGB composite images of the study areas before and after the disturbances. GEDI and ATLAS footprints are overlaid on these images to illustrate surface height variations and scene changes. Near vertical patterns represent ATLAS footprints, while the slanted lines correspond to GEDI data. The surface relative height in the first area ranges from 0 to 30 metres, while the second area exhibits a maximum height of approximately 60 metres.

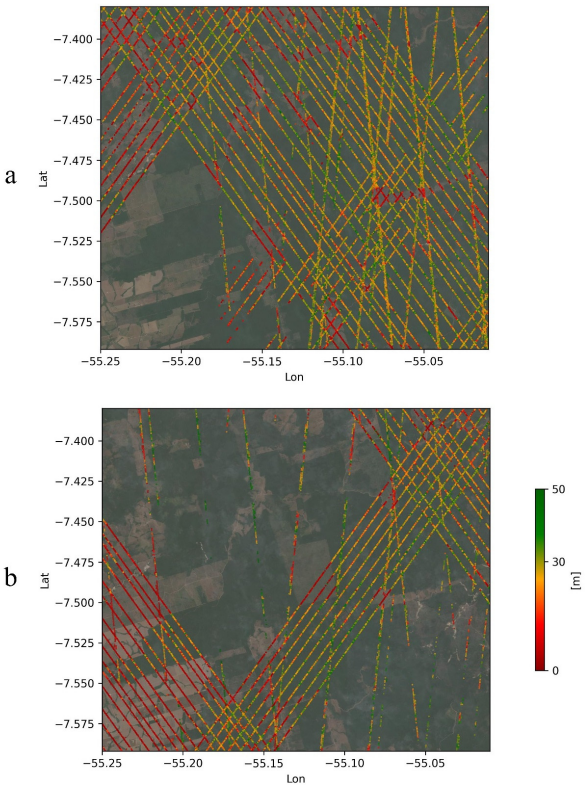

Figure 2: The second study area is in Brazil: a) Before and b) After the changes. Slanted and near-vertical patterns demonstrate height measurements by GEDI and ATLAS LiDARs, respectively.

4. Results and Discussion

As detailed in Section 2.1, this study utilises three types of data for forest change mapping: SAR backscatter (Sentinel-1), Multispectral (Sentinel-2), and LiDAR canopy height data (GEDI L2A and ICESat-2 ATL08). While the first two data sources consist of gridded image arrays, the canopy height data is in point cloud format distributed across different parts of the study areas.

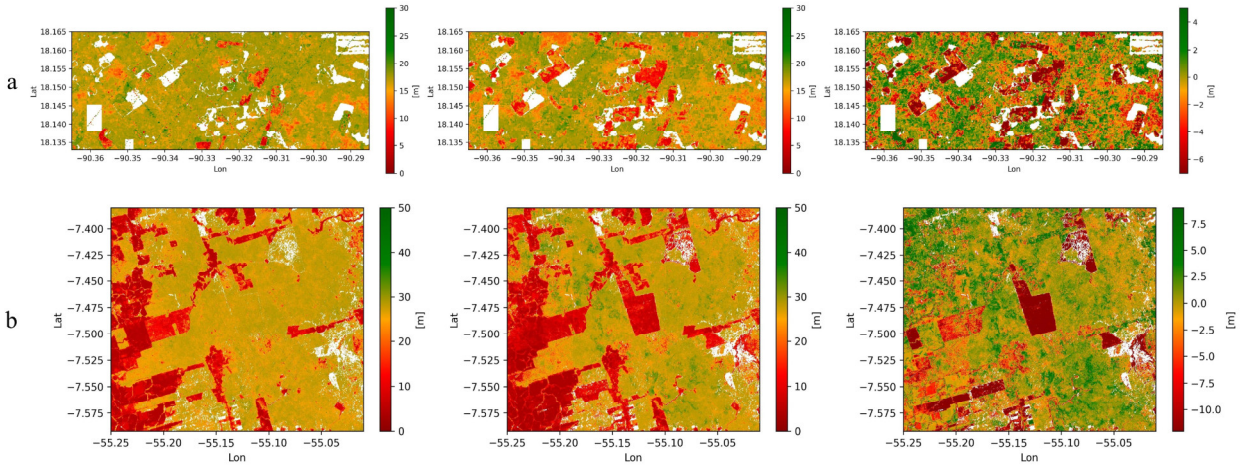

Figure 3: Extrapolated height images: a) First area, b) Second area. The top, middle, and bottom images represent extrapolated images from time-1, time-2, and their difference, respectively.

This contribution has been peer-reviewed. The double-blind peer-review was conducted on the basis of the full paper.
https://doi.org/10.5194/isprs-annals-X-4-2024-163-2024 | © Author(s) 2024. CC BY 4.0 License.

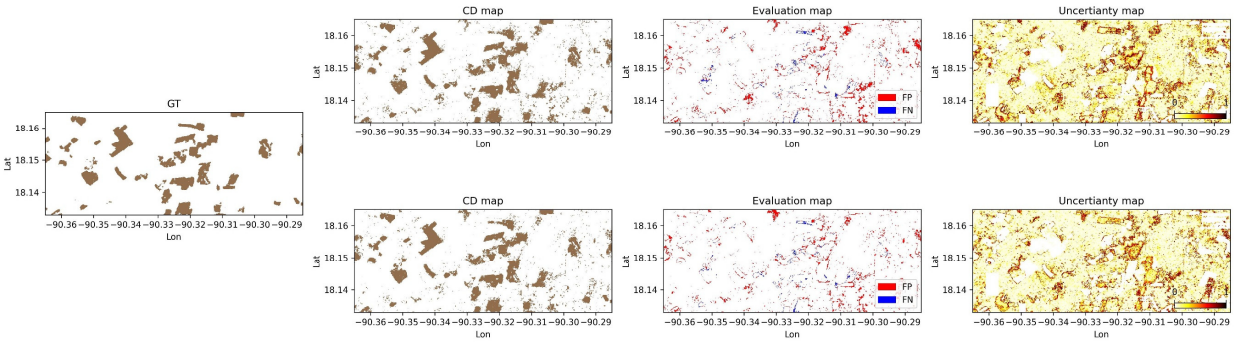

a b c d

Figure 4: Change maps of the first study area (Up: using only SAR and optical features. Bottom: incorporating canopy height into the image features): a) Ground truth, b) Estimated change map, c) Spatial distribution of false positive (FP) and false negative (FN) pixels, d) Model uncertainty.

As can be seen from Figure 1 and Figure 2, the height measurements are sparsely distributed across each scene, and many of the 10×10m pixels lack height measurements. To address this issue, we extrapolated height measurements by creating a Random Forest Regression model. This model uses the Sentinel-2 spectral bands and Sentinel-1 VV and VH intensity images as input variables to estimate the canopy height of each pixel. We utilised 200 tree estimators with a model depth 10 for all scenes. The modelling results are presented in Table 1, showing that the mean absolute errors of the models range between 2 to 5 metres.

Study region	Time-1 (m)	Time-2 (m)
Area-1	2.766	2.316
Area-2	5.118	4.776

Table 1: Mean absolute error of canopy height extrapolation modelling.

Finally, each scene’s wall-to-wall 10m resolution canopy height image is demonstrated in Figure 3. The generated images reveal noticeable height changes in both scenes, with most changes appearing negative (indicating a decrease in height), while some areas show slight increases or growth. These generated height maps serve as a feature layer for change detection modelling alongside other features derived from SAR and optical imagery.

Seven feature layers were extracted from four remotely sensed datasets used in this study. These include three indices (NDVI, SAVI, and NBR) from the Sentinel-2 multispectral imagery, three features (Span, Ratio, and RVI) from the Sentinel-1 dual-polarised GRD data, and the canopy height measurements from LiDAR, for each period.

We employed a Random Forest Classifier with 200 estimators and a depth of 10 to identify change and no-change areas. This model was trained on feature layers derived by subtracting corresponding layers from time 1 and time 2 for each data source.

Figures 4b and 5b present the generated change maps for the first and second areas. These maps depict the results of two modelling scenarios: one using only features derived from SAR and multispectral data, and another incorporating the canopy height feature layer. Overall, both scenarios agreed well with the reference maps, correctly identifying major changes. However,

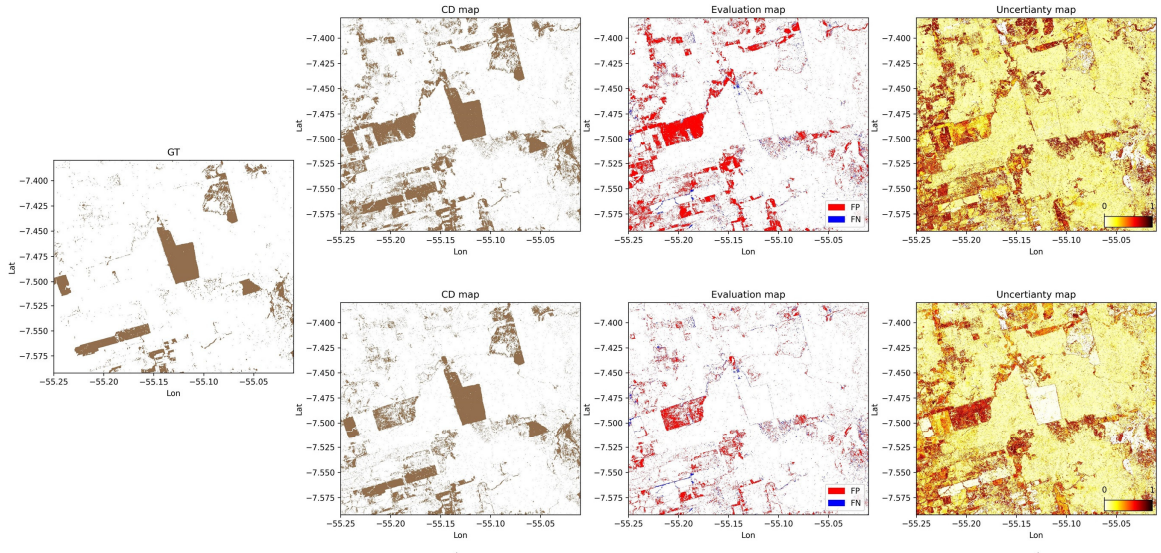

a b c d

Figure 5: Change maps of the first study area (Up: using only SAR and optical features. Bottom: incorporating canopy height into the image features): a) Ground truth, b) Estimated change map, c) Spatial distribution of false positive (FP) and false negative (FN) pixels, d) Model uncertainty.

This contribution has been peer-reviewed. The double-blind peer-review was conducted on the basis of the full paper.
https://doi.org/10.5194/isprs-annals-X-4-2024-163-2024 | © Author(s) 2024. CC BY 4.0 License.

the first scenario (without height data) exhibited a higher prevalence of false detections and errors (Figures 4c and 5c). Notably, including the height feature layer improved detection precision (user’s accuracy) in the first area from 0.66 to 0.7 and in the second area from 0.40 to 0.55 (Table 2). Furthermore, the F-score for change detection increased by 0.03 and 0.13 in the two areas when height information was included, further emphasising its effectiveness in forest change mapping.

We analysed the model’s uncertainty in detecting changes to assess its performance further. This involved estimating the probability of the predicted label for each pixel during the testing phase. A higher uncertainty score (calculated using the formula $2(1-\hat{p}_i)$, where $\hat{p}_i \in \mathbb{R}^{[0.5,\ 1]}$ is the model’s label prediction probability for the i^{th} pixel) indicates lower model confidence in the prediction. As illustrated in Figures 4d and 5d, the model without the height feature layer exhibited lower sensitivity to prediction uncertainty. In contrast, including the height layer improved the model’s confidence in correctly identifying changes while assigning higher uncertainty to incorrect predictions. For example, in Figure 5d, the base model shows similar confidence levels for correctly and incorrectly predicted changes in the central area. However, when height information was included, the model’s uncertainty decreased for correctly predicted changes and increased for incorrectly predicted changes.

Study Region	Method	Precision	Recall	F-1
#1	S1, S2	0.66	0.94	0.78
#1	S1, S2, H	0.70	0.94	0.81
#2	S1, S2	0.40	0.88	0.55
#2	S1, S2, H	0.55	0.89	0.68

Table 2. Change detection results (S1, S2, and H represent features from Sentinel-1, Sentinel-2, and canopy heights from GEDI and ATLAS, respectively).

To evaluate change detection based solely on the predicted change probability ($\hat{p}^c$), we analysed Precision-Recall curves for each scenario (Figure 6). The impact of including the height layer is demonstrated in both study areas, as evidenced by an increase in the area under the curve (AUC) from 0.9042 to 0.9278 for the first study area and from 0.7245 to 0.8479 for the second study area. These results highlight the enhancement in the model’s confidence in accurately detecting changes.

A more precise model uncertainty estimation can offer valuable insights for developing advanced modelling approaches. These approaches could include human-in-the-loop active learning for manually labelling pixels with low prediction confidence or pseudo-label propagation based on semi-supervised methods (Hosseiny et al., 2023).

Figure 7 illustrates the distributions of extracted features for changed and unchanged areas. Notably, the discriminability between distributions is less evident in features derived from SAR data. This might be attributed to the complex backscattering behaviour of forests, particularly related to volume, which dual-polarised intensity data cannot fully capture. However, the distance between the medians of unchanged and changed pixels is most distinctive in the SAR Span layer. This could be explained by transforming volume or dihedral backscattering in forested areas to surface scattering after disturbance, significantly reducing backscattering power for VV and VH polarisations.

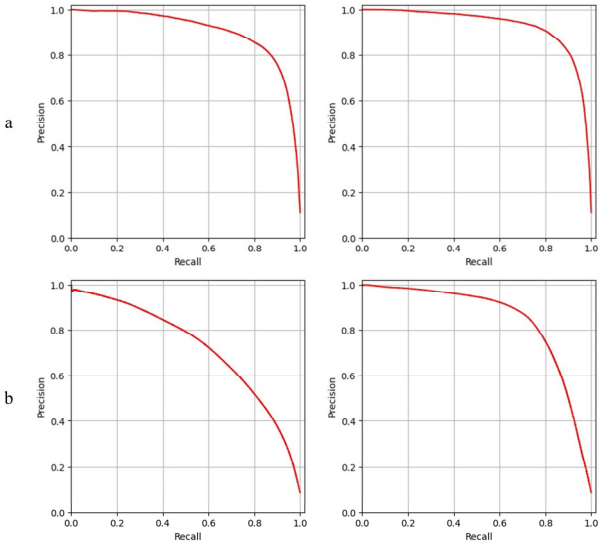

Figure 6: Precision-Recall curve for detecting change pixels (Left: using only SAR and optical features. Right: incorporating canopy height into the image features): a) First study area, b) Second study area.

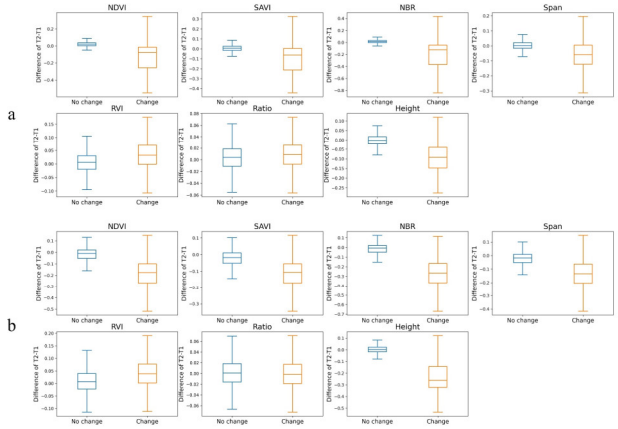

Figure 7: Feature distributions: a) First study area, b) Second study area (note that the height values are normalised between -1 and 1 to have the same scale as the other features).

Spectral features from Sentinel-2 show better discrimination, with no-change areas exhibiting a concentrated distribution. NDVI and SAVI are both sensitive to surface greenness. NBR, which utilises shortwave infrared reflectivity, offers further sensitivity to disturbances like forest fires or changes in general vegetation health. Since these spectral indices rely on the physical characteristics of the observed media, capturing data under similar conditions and vegetation cycles is likely to yield similar results in unchanged areas. However, as observed, the distribution of changed pixels is wider.

The height layer also displays a wide standard deviation for changed pixels, reflecting the complexity of forest changes. However, compared to SAR and optical features that provide insights about surface appearance and physical characteristics, the height feature directly compares changes in the vertical direction. This feature provides more distinctiveness between the medians of unchanged and changed pixel distributions.

This contribution has been peer-reviewed. The double-blind peer-review was conducted on the basis of the full paper.
https://doi.org/10.5194/isprs-annals-X-4-2024-163-2024 | © Author(s) 2024. CC BY 4.0 License.

5. Conclusion

This study investigated the effectiveness of multi-source satellite remote sensing for forest change mapping, focusing on the impact of incorporating canopy height information. We presented a processing framework that integrates features derived from Sentinel-1 (SAR), Sentinel-2 (optical), and GEDI/ICESat-2 (canopy height) data. Experiments were conducted in two study areas in Mexico and Brazil, which experienced severe disturbances and deforestation during 2020-2021. The results demonstrated that incorporating canopy height features improves forest change mapping accuracy. Compared to models relying solely on SAR and optical data, our approach achieved a 15% and 13% improvement in precision and F1 scores, respectively. Notably, the canopy height layer discriminates better between changed and unchanged pixels than other feature layers.

Additionally, analyses of the model’s prediction confidence revealed a considerable increase in confidence for correctly classified pixels and a decrease for incorrect predictions. These findings highlight the value of multi-source satellite remote sensing for forest change monitoring. Combining data from different sensors provided a more comprehensive picture of forest dynamics, leading to more accurate change detection. Specifically, canopy height measurements emerged as a key factor in boosting model accuracy. The potential reactivation of the GEDI instrument by the end of 2024, along with continued data collection from optical and SAR sensors, offers a promising avenue for establishing a more accurate and frequent forest monitoring and change detection system.

Acknowledgements

The authors would like to express their sincere gratitude to Dr. Pouria Ramzi for his invaluable support, and insightful comments throughout the development of this paper.

References

Adeli, S., Quackenbush, L.J., Salehi, B., Mahdianpari, M., 2023. GEDI and Sentinel-2 Integration for Mapping Complex Wetlands. In: IGARSS 2023 - *2023 IEEE International Geoscience and Remote Sensing Symposium*, IEEE, pp. 5635–5637.

Di Tommaso, S., Wang, S., Lobell, D.B., 2021. Combining GEDI and Sentinel-2 for wall-to-wall mapping of tall and short crops. *Environ. Res. Lett.* 16, 125002.

Dubayah, R., Blair, J.B., Goetz, S., Fatoyinbo, L., Hansen, M., Healey, S., Hofton, M., Hurtt, G., Kellner, J., Luthcke, S., 2020. The global ecosystem dynamics investigation: High-resolution laser ranging of the Earth’s forests and topography. *Sci. Remote Sens.*, 1, 100002. doi.org/10.1016/j.srs.2020.100002

Feng, T., Duncanson, L., Montesano, P., Hancock, S., Minor, D., Guenther, E., Neuenschwander, A., 2023. A systematic evaluation of multi-resolution ICESat-2 ATL08 terrain and canopy heights in boreal forests. *Remote Sens. Environ.,*291, 113570.

Hosseiny, B., Mahdianpari, M., Hemati, M., Radman, A., Mohammadimanesh, F., Chanussot, J., 2023. Beyond supervised learning in remote sensing: A systematic review of deep learning approaches. *IEEE J. Sel. Top. Appl. Earth Obs. Remote Sens.*, pp. 1–22. doi.org/10.1109/JSTARS.2023.3316733

Kim, Y., Zyl, J.J. van, 2009. A time-series approach to estimate soil moisture using polarimetric radar data. *IEEE Trans. Geosci. Remote Sens.*, 47(8), pp. 2519–2527., doi.org/10.1109/TGRS.2009.2014944

Liu, A., Cheng, X., Chen, Z., 2021. Performance evaluation of GEDI and ICESat-2 laser altimeter data for terrain and canopy height retrievals. *Remote Sens. Environ.*, 264, 112571.

Mandal, D., Kumar, V., Ratha, D., Dey, S., Bhattacharya, A., Lopez-Sanchez, J.M., McNairn, H., Rao, Y.S., 2020. Dual polarimetric radar vegetation index for crop growth monitoring using sentinel-1 SAR data. *Remote Sens. Environ.*, 247, 111954.

Milenković, M., Reiche, J., Armston, J., Neuenschwander, A., De Keersmaecker, W., Herold, M., Verbesselt, J., 2022. Assessing Amazon rainforest regrowth with GEDI and ICESat-2 data. *Sci. Remote Sens.,* 5, 100051.

Neuenschwander, A., Pitts, K., Jelley, B., Robbins, J., Markel, J., Popescu, S., Ross, N., Harding, D., Pederson, D., Klotz, B., Sheridan, R., 2022. *Ice, Cloud, and Land Elevation Satellite (ICESat-2) Project Algorithm Theoretical Basis Document (ATBD) for Land - Vegetation Along-Track Products (ATL08),* Version 6. ICESat-2 Project. doi.org/10.5067/8ANPSL1NN7YS

Neumann, T.A., Martino, A.J., Markus, T., Bae, S., Bock, M.R., Brenner, A.C., Brunt, K.M., Cavanaugh, J., Fernandes, S.T., Hancock, D.W., 2019. The Ice, Cloud, and Land Elevation Satellite–2 Mission: A global geolocated photon product derived from the advanced topographic laser altimeter system. Remote Sens. Environ., 233, 111325.

Qi, W., Armston, J., Choi, C., Stovall, A., Saarela, S., Pardini, M., Fatoyinbo, L., 2023. Mapping large-scale pantropical forest canopy height by integrating GEDI LiDAR and TanDEM-X InSAR data. PREPRINT (Version 1) available at Research Square. doi.org/10.21203/rs.3.rs-3306982/v1

Reiche, J., Mullissa, A., Slagter, B., Gou, Y., Tsendbazar, N.-E., Odongo-Braun, C., Vollrath, A., Weisse, M.J., Stolle, F., Pickens, A., 2021. Forest disturbance alerts for the Congo Basin using Sentinel-1. Environ. Res. Lett., 16, 024005.

Slagter, B., Reiche, J., Marcos, D., Mullissa, A., Lossou, E., Peña-Claros, M., Herold, M., 2023. Monitoring direct drivers of small-scale tropical forest disturbance in near real-time with Sentinel-1 and-2 data. *Remote Sens. Environ.*, 295, 113655.

Tamiminia, H., Salehi, B., Mahdianpari, M., Goulden, T., 2024. State-wide forest canopy height and aboveground biomass map for New York with 10 m resolution, integrating GEDI, Sentinel-1, and Sentinel-2 data. Ecol. Inform., 79, 102404.

Vogt, P., Riitters, K.H., Caudullo, G., Eckhardt, B., 2019. FAO-State of the World’s Forests: Forest Fragmentation. Publications Office of the European Union: Luxembourg.

Zanaga, D., Van De Kerchove, R., Daems, D., De Keersmaecker, W., Brockmann, C., Kirches, G., Wevers, J., Cartus, O., Santoro, M., Fritz, S., 2022. ESA WorldCover 10 m 2021 v200. doi.org/10.5281/zenodo.7254221